

## HIGH-RESOLUTION LAMB DIP SPECTROSCOPY ON OD AND SiCl IN A MOLECULAR BEAM

Gerard MEIJER, Wim UBACHS<sup>1</sup>, J.J. TER MEULEN and A. DYMANUS

*Department of Molecular and Laser Physics, Katholieke Universiteit Nijmegen,  
Toernooiveld, 6525 ED Nijmegen, The Netherlands*

Received 26 May 1987

High-resolution Lamb dip spectra of OD and Si<sup>35</sup>Cl have been observed in a molecular beam. The Lamb dips of OD have a width (fwhm) of 1.5 MHz. For Si<sup>35</sup>Cl broader Lamb dips were seen; from this broadening the radiative lifetime  $\tau_r = 8-10$  ns of individual rotational levels of the B<sup>2</sup> $\Sigma^+$ ,  $v' = 0$  state was determined. The hyperfine structure of the rotational transitions could be resolved and explained by the hyperfine splitting of the ground state only.

### 1. Introduction

In many high-resolution molecular beam studies based on laser-induced fluorescence (LIF), the resolution is limited by the residual Doppler broadening caused by the divergence of the molecular beam. A stronger collimation of the molecular beam to reduce this Doppler broadening is limited by a large loss in the beam intensity. To overcome this problem we applied a Doppler-free Lamb dip detection technique, as also used by Kröckertskothén et al. [1], which allows use of a wide, intense molecular beam. General features of this technique as well as the high resolution that can be obtained are experimentally demonstrated for the OD radical. In this radical the well-known A<sup>2</sup> $\Sigma^+$ ,  $v' = 0 \leftarrow X^2\Pi$ ,  $v'' = 0$  transition around 308 nm is induced, using the narrow bandwidth radiation from a cw intra-cavity frequency-doubled ring-dye laser. For the first time the hyperfine splittings of OD in the A<sup>2</sup> $\Sigma^+$  state could be measured directly by LIF. The resulting hyperfine constants are in agreement with the previous values obtained by German from high-field level crossing spectroscopy [2].

The same method is then applied to the B<sup>2</sup> $\Sigma^+$ ,  $v' = 0 \leftarrow X^2\Pi$ ,  $v'' = 1$  transition of the SiCl radical around 296–299 nm. In a previous paper [3] we reported an extensive analysis of the rotational structure of this transition observed with the normal LIF technique. With the Lamb dip detection technique the splittings due to the hyperfine interactions could be resolved. For the upper B<sup>2</sup> $\Sigma^+$ ,  $v' = 0$  state the hyperfine splitting is very small, and only an upper limit for the hyperfine constants could be given. From the widths of the Lamb dips of single hyperfine transitions the natural lifetime of the SiCl B<sup>2</sup> $\Sigma^+$ ,  $v' = 0$  state is determined. It is shown that this technique can be used to determine lifetimes of excited states that lie in the 0.1–20 ns region, a region not easily accessible to other techniques.

### 2. Experimental

The experimental arrangement is schematically shown in fig. 1. The radicals are produced in a coaxial microwave discharge cavity [4]. For the production of OD a discharge in pure D<sub>2</sub>O ( $\geq 99.9\%$ ) is used, whereas for SiCl the discharge is induced in a 10 to 1 mixture of Ar and SiCl<sub>4</sub> [3]. The beam orifice is a cylindrical hole

<sup>1</sup> Present address: Department of Chemistry, Stanford University, Stanford, CA 94305, USA.

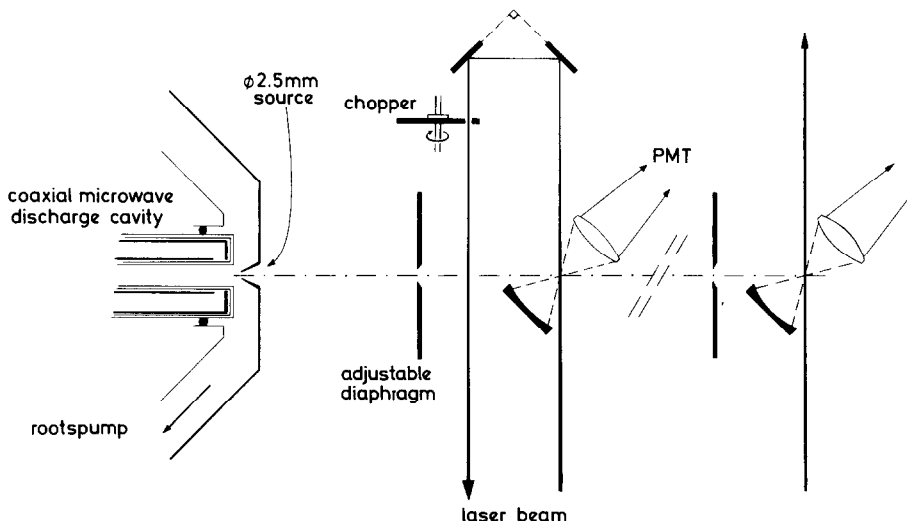


Fig. 1. Scheme of the experimental arrangement.

(2.5 mm diameter) in a brass plate. Three differentially pumped vacuum chambers with adjustable diaphragms in between form the molecular beam machine.

The LIF detection region is about 15 cm away from the beam orifice. Here the UV laser beam crosses the molecular beam perpendicularly and fluorescence produced in this point is imaged on a photomultiplier tube (PMT). The transmitted laser beam is reflected by two mirrors such as to intersect the molecular beam again at about 4.5 cm upstream of the probing region. Fluorescence produced in this crossing point cannot reach the PMT. By optical pumping in this point a certain angular fraction of molecules in a given state is partly transferred to other states. A hole is burned in the angular distribution in the molecular beam, which is detected as a Lamb dip by the counter-propagating probe beam, when the frequency is swept. In this arrangement it is possible to modulate the pump laser beam by means of a mechanical chopper and to detect the Lamb dip against a flat base line, using normal lock-in detection. The chopping frequency is about 400 Hz.

There is also a second LIF detection region, about 70 cm away from the beam orifice, where the molecular beam is better collimated. In this region resolved hyperfine transitions starting from the lowest rotational levels of the  $X^2\Pi$ ,  $v''=1$  state of SiCl were observed. These transitions were too weak to be detected by the Lamb dip technique.

The UV radiation is obtained by frequency doubling in a  $\text{LiIO}_3$  crystal inside the cavity of a single-frequency ring-dye laser [5], operating on rhodamine 6G. A typical UV power of 1–2 mW single mode scannable over 80 GHz and with a bandwidth of about 0.5 MHz (rms) is obtained. To avoid additional broadening effects the UV laser is only very weakly focused, having a divergence of less than 0.2 mrad. The spectra were recorded together with the markers of a pressure and temperature stabilized interferometer with a free spectral range of  $148.40 \pm 0.07$  MHz.

### 3. OD spectra

First we recorded Lamb dip spectra of OD, inducing several rotational transitions in the  $A^2\Sigma^+$ ,  $v'=0 \leftarrow X^2\Pi$ ,  $v''=0$  band [6], around 308 nm. We did not expect to obtain new spectroscopic data for this radical, but just used it to show some general features of the Lamb dip technique. The radical is perfectly suited for this purpose because it can easily be produced and detected with a good signal-to-noise ratio in our arrangement. Fur-

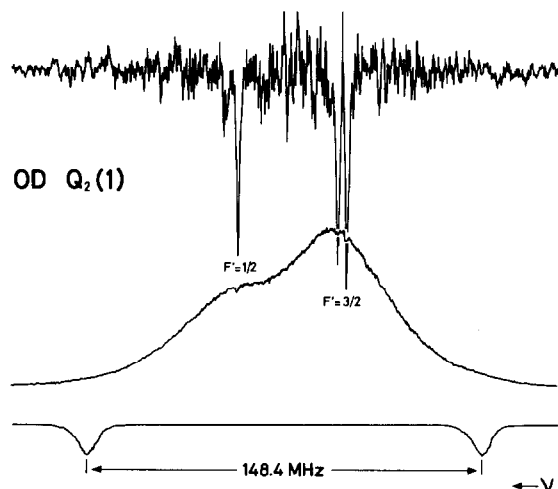


Fig. 2. Recording of the  $Q_2(1)$  transition of OD. In the upper curve single resolved hyperfine transitions with a width of 1.5 MHz (fwhm) are seen.

thermore, the lifetime of the excited  $A^2\Sigma^+$ ,  $v'=0$  state is well known [7] and is long enough to give an almost negligible contribution to the linewidth of the Lamb dips. Therefore this molecule makes it possible to determine the influence of other, especially the geometrical, broadening effects.

A recording of the  $Q_2(1)$  transition ( $A^2\Sigma^+$ ,  $N'=1$ ,  $J'=1/2 \leftarrow X^2\Pi_{1/2}$ ,  $N''=1$ ,  $J''=1/2$ ) of OD is shown in fig. 2. The lowest trace shows the relative frequency scale, as given by the transmission peaks of the interferometer. The recording in the middle shows the direct LIF signal of the  $Q_2(1)$  transition. This transition consists of several hyperfine components that are almost completely overlapped due to the residual Doppler broadening of almost 50 MHz. When one looks very carefully, Lamb dips can be recognized on top of this curve. These dips only amount to about 4% of the total signal. In the upper spectrum the Lamb dips are seen against a flat base-line, using the forementioned lock-in detection technique. The noise in the upper curve is mainly due to the statistical noise in the direct signal itself. The three strongest of the four expected hyperfine transitions are seen, the fourth one being more than an order of magnitude weaker. The transitions are indicated in fig. 2 by the total quantum number  $F=J'+I'$  in the final state. The two hyperfine transitions going to the  $F'=3/2$  level are separated exactly by the hyperfine splitting in the  $X^2\Pi_{1/2}$ ,  $J''=1/2$  level. This splitting, completely resolved in the Lamb dip spectrum, is known from microwave spectroscopy to be about 3.39 MHz [8].

It should be mentioned that the Lamb dip is positioned at  $\nu_0$ , the frequency of the molecular transition, as long as the pump and probe laser beam are exactly anti-parallel. This is independent of the angle that the laser beams make with the molecular beam axis, provided this angle is smaller than the divergence angle of the molecular beam. If on the other hand the pump and probe laser beam make a certain angle  $2\theta$ , the Lamb dip is shifted away from  $\nu_0$ , because it is produced by molecules which make an angle of  $90^\circ + \theta$  with both laser beams.

The width of individual Lamb dips, consisting of single hyperfine transitions, is about 1.5 MHz. This corresponds with a spectral resolution of  $7 \times 10^8$  which is an order of magnitude larger than we could obtain by a stronger collimation of the molecular beam [4]. The observed linewidth of 1.5 MHz is due to several effects. First, there is the homogeneous linewidth of about 0.2 MHz due to the finite lifetime of the  $A^2\Sigma^+$ ,  $v'=0$  state [7], which is the ultimate resolution limit. Second, there are geometrical broadening effects which depend strongly on the focusing of the laser. These effects include the divergence of the laser beam, transit-time broadening and broadening due to the curvature of the wavefront. For a short interaction region between the molecules and the laser radiation, the transit-time broadening is large whereas for a longer interaction region, away from the focus, the curvature of the wave restricts the effective transit time and broadens the line [9]. As a compromise between these two effects a laser beam diameter at the molecular beam crossing points of about 1 mm is chosen, from which an additional broadening of only 0.4 MHz is expected. The divergence of the laser beam is less than 0.2 mrad, which means there is left a residual Doppler broadening of less than 0.9 MHz,

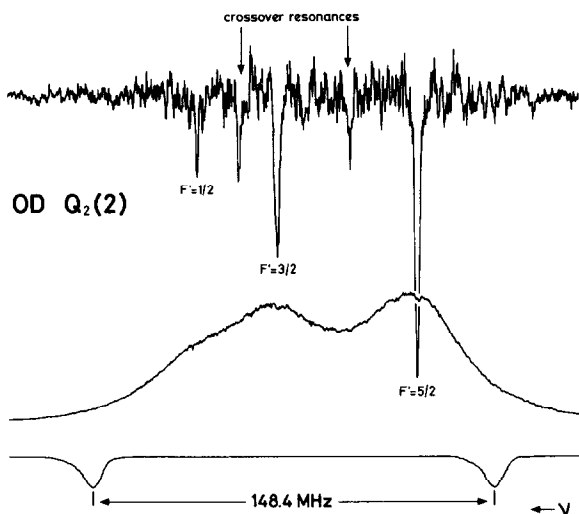


Fig. 3. Recording of the  $Q_2(2)$  transition of OD. Halfway between the Lamb dips, which now consist of several overlapping hyperfine transitions, cross-over resonances are seen.

assuming a most probable velocity in the beam of  $v_p = 800$  m/s [10]. Another broadening effect is due to the fast frequency jitter of the laser of about 0.5 MHz. Power broadening can clearly be neglected because the dips are very small compared with the direct signal. Another indication that it is justified to neglect power broadening is the observation that the intensity of the Lamb dip signal depends quadratically on the applied laser power, for the powers we used.

In fig. 3 the  $Q_2(2)$  transition of OD is shown. The three peaks indicated by the  $F'$  quantum number of the final state all consist of several unresolved hyperfine transitions; the hyperfine splitting in the ground state is too small to be resolved [8], and only some broadening of the Lamb dips is seen. Halfway between these peaks additional peaks due to so-called cross-over resonances [9] are seen. These resonances are caused by molecules making two different transitions from the same initial state, so by molecules making different angles with the two laser beams. This means the cross-over resonances are produced by molecules making a certain angle with the molecular beam axis, and can be suppressed by a better collimation of the molecular beam.

To determine the hyperfine splitting in the  $A^2\Sigma^+$ ,  $v' = 0$  state of OD several rotational transitions were measured using this Lamb dip technique. The magnetic hyperfine splitting in a  $^2\Sigma$  state due to a nucleus with nuclear spin  $I$  can be described by the Hamiltonian:

$$H_{\text{hfs}} = b\mathbf{I} \cdot \mathbf{S} + cI_z S_z, \quad (1)$$

where  $b$  and  $c$  are the Frosch and Foley [11] parameters and  $\mathbf{S}$  is the resultant electronic spin angular momentum. On the basis of pure Hund's case b wavefunctions  $|^2\Sigma^+ N S J I F\rangle$  in the coupling scheme  $\mathbf{J} = \mathbf{N} + \mathbf{S}$ ,  $\mathbf{F} = \mathbf{J} + \mathbf{I}$  the matrix elements of the hyperfine Hamiltonian (1) are

$$\begin{aligned} \langle ^2\Sigma^+ N J = N + \frac{1}{2} I F | H_{\text{hfs}} | ^2\Sigma^+ N J = N + \frac{1}{2} I F \rangle &= \frac{F(F+1) - (N + \frac{1}{2})(N + \frac{3}{2}) - I(I+1)}{4(N + \frac{1}{2})} \left( b + \frac{c}{2N+3} \right), \\ \langle ^2\Sigma^+ N J = N - \frac{1}{2} I F | H_{\text{hfs}} | ^2\Sigma^+ N J = N - \frac{1}{2} I F \rangle &= \frac{F(F+1) - (N - \frac{1}{2})(N + \frac{1}{2}) - I(I+1)}{4(N + \frac{1}{2})} \left( -b + \frac{c}{2N-1} \right), \\ \langle ^2\Sigma^+ N J = N - \frac{1}{2} I F | H_{\text{hfs}} | ^2\Sigma^+ N J = N + \frac{1}{2} I F \rangle &= - \frac{[(F+I+N+\frac{3}{2})(I+N+\frac{1}{2}-F)(F+N+\frac{1}{2}-I)(F+I+\frac{1}{2}-N)]^{1/2}}{4(N + \frac{1}{2})} (2b + \frac{1}{2}c). \end{aligned} \quad (2)$$

Table 1

Observed and calculated hyperfine splittings in the  $A^2\Sigma^+$ ,  $v'=0$  state of OD. The observed splittings are already corrected for the small hyperfine splitting in the ground state [8]. In the last column the observed minus calculated values are given. The values of the hyperfine constants  $b$  and  $c$  obtained here in a least-squares fit are  $b=109.4\pm 0.6$  and  $c=25.9\pm 1.5$ , to be compared with the values  $b=109.73\pm 0.10$  and  $c=25.73\pm 0.25$  obtained by German [2]

| $N'$ | $J'$ | Observed splitting (MHz)<br>$F'_{\text{upper}}-F'_{\text{lower}}$ | Obs. - calc. |
|------|------|---|--------------|
| 1    | 1/2  | $F' = 1/2 - F' = 3/2$ 42.6 ± 0.8                                  | -0.05        |
| 2    | 3/2  | $F' = 1/2 - F' = 3/2$ 30.6 ± 1.4                                  | -0.24        |
|      |      | $F' = 3/2 - F' = 5/2$ 50.8 ± 1.3                                  | 0.09         |
| 2    | 5/2  | $F' = 7/2 - F' = 5/2$ 76.9 ± 1.5                                  | -1.36        |
|      |      | $F' = 5/2 - F' = 3/2$ 57.8 ± 1.3                                  | 0.91         |
| 3    | 5/2  | $F' = 3/2 - F' = 5/2$ 38.7 ± 1.5                                  | 0.98         |
|      |      | $F' = 5/2 - F' = 7/2$ 52.4 ± 1.0                                  | 0.12         |
| 4    | 7/2  | $F' = 5/2 - F' = 7/2$ 42.0 ± 0.7                                  | 0.49         |
|      |      | $F' = 7/2 - F' = 9/2$ 52.7 ± 0.6                                  | -0.26        |

The minor effect of the interaction between states with  $\Delta N=2$  is omitted. The contribution to the hyperfine Hamiltonian due to the interaction of the quadrupole moment of the D nucleus was neglected in view of the experimental accuracy obtained. The energies of the hyperfine levels for every rotational level  $N$  can be calculated by rearranging matrix elements in  $2 \times 2$  matrix blocks for each  $F$ -level, that can easily be diagonalized. Therefore only the spin-rotation interaction ( $\gamma N \cdot S$ ) has to be added to the Hamiltonian (1).

The observed splittings were corrected for the hyperfine splitting in the  $X^2\Pi$ ,  $v''=0$  ground state [8] and are given in table 1. The magnetic hyperfine parameters  $b$  and  $c$  were determined in a least-squares fit using the formulae (2) with  $I=1$  for the D nucleus. For the spin-rotation interaction the constant  $\gamma=0.1201 \text{ cm}^{-1}$  as given by Coxon [12] is used. As can be seen from table 1 the present constants are in agreement with the constants known from high-field level crossing spectroscopy [2], but they are less accurate. This is due to the fact that the accuracy in the determination of the frequency distance between individual hyperfine components is limited by the non-linearity of the laser scan. This means that splittings could "only" be measured with an accuracy of about 1-2 MHz. With an improved linearity of the scan we expect an accuracy in the order of 100 kHz.

#### 4. SiCl spectra

The rotational and fine structure in both the  $X^2\Pi$ ,  $v''=1$  and  $B^2\Sigma^+$ ,  $v''=0$  of  $\text{Si}^{35}\text{Cl}$  has been treated extensively in ref. [3]. This treatment has to be supplemented by that of the hyperfine structure which could be resolved in the present experiment. The magnetic hyperfine and quadrupole interaction in the  $X^2\Pi$  state is due to the nuclear spin  $I=3/2$  of the chlorine nucleus. These interactions can be described by the Hamiltonians [13,14]:

$$H_{\text{hfs}} = aI_zL_z + b\mathbf{I} \cdot \mathbf{S} + cI_zS_z + \frac{1}{2}d(e^{-2i\phi}I_+S_+ + e^{2i\phi}I_-S_-) \quad (3)$$

and

$$H_Q = eqQ(3I_z^2 - I^2)/4I(2I-1), \quad (4)$$

where  $a$ ,  $b$ ,  $c$  and  $d$  are the Frosch and Foley [11] parameters. The constant  $eqQ$  is the quadrupole coupling parameter,  $L$  and  $S$  are the resultant electronic orbital and spin angular momentum, respectively, and  $\phi$  is the electron orbital azimuthal coordinate with respect to the internuclear axis. Hyperfine matrix elements can be calculated using symmetrized Hund's case a wavefunctions [3] for the  $X^2\Pi$  state. In a first approximation

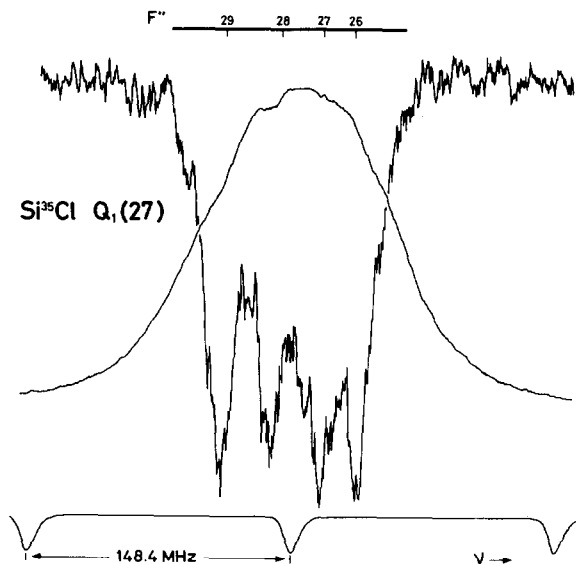


Fig. 4. Recording of the  $Q_1(27)$  transition of  $\text{Si}^{35}\text{Cl}$ . The width of the individual hyperfine transitions is about 20 MHz, due to the short lifetime of the  $\text{B}^2\Sigma^+$ ,  $v'=0$  state. The positions of the  $\Delta F=0$  hyperfine transitions when neglecting the hyperfine splitting in the excited state and assuming the same hyperfine splitting for  $v''=1$  as for  $v''=0$  in the ground state, are indicated on the bar in the upper part of the figure by the  $F''$  quantum number of the ground state.

the interaction between levels with a different  $J$  quantum number can be neglected. As the ground state of  $\text{SiCl}$  is almost pure Hund's case a ( $A/B \approx 815$ ), the mixing between different spin multiplets can also be neglected. In this approximation the hyperfine splitting in each of the  ${}^2\Pi_{\Omega}$  multiplets is directly given by:

$$\begin{aligned} & \langle {}^2\Pi_{1/2}, JF \pm | H_{\text{hfs}} + H_Q | {}^2\Pi_{1/2}, JF \pm \rangle \\ &= \frac{K}{2J(2J+2)} \left[ \left( a - \frac{b+c}{2} \right) \mp (J + \frac{1}{2})d \right] + \frac{eqQ}{4} \frac{2 \left[ \frac{3}{4} - J(J+1) \right] [K(K+1) - 5J(J+1)]}{(2J-1)(2J)(2J+2)(2J+3)}, \\ & \langle {}^2\Pi_{3/2}, JF \pm | H_{\text{hfs}} + H_Q | {}^2\Pi_{3/2}, JF \pm \rangle \\ &= \frac{K}{2J(2J+2)} \left[ 3 \left( a + \frac{b+c}{2} \right) \right] + \frac{eqQ}{4} \frac{2 \left[ \frac{7}{4} - J(J+1) \right] [K(K+1) - 5J(J+1)]}{(2J-1)(2J)(2J+2)(2J+3)}, \end{aligned} \quad (5)$$

with  $K = F(F+1) - J(J+1) - 15/4$ .

As the different hyperfine constants for the  $\text{X}^2\Pi$ ,  $v''=1$  state are not known, we use the constants for the  $v''=0$  state [13] as a first approximation to estimate the splittings. For large values of  $J$  only the  $d$  constant ( $\approx 46$  MHz [15]) and, for a minor part, the electric quadrupole interaction term ( $eqQ \approx -23$  MHz [15]) give a considerable contribution to the splitting. As a consequence the splitting in the  ${}^2\Pi_{1/2}$  multiplet is much larger than the splitting in the  ${}^2\Pi_{3/2}$  multiplet for high  $J$  values.

The magnitude of the hyperfine splitting in the  $\text{B}^2\Sigma^+$  state is estimated from eqs. (2) with  $I=3/2$ , neglecting the minor effect of the interaction between different spin-doublet components. It is then seen from eqs. (2) that for high  $N$  values the splitting in different  $F$  levels is mainly determined by the magnetic hyperfine constant  $b$ . The  $c$  constant can only be determined from the hyperfine splitting in states with a low  $N$  value.

A typical  $\text{B}^2\Sigma^+$ ,  $v'=0 \leftarrow \text{X}^2\Pi_{1/2}$ ,  $v''=1$  LIF transition of  $\text{Si}^{35}\text{Cl}$  is shown in fig. 4. The upper curve is the curve obtained with phase-sensitive detection and clearly shows four peaks. The curve in the middle is the direct LIF signal on which the Lamb dips are hardly visible. Nevertheless the decrease of the direct signal on a Lamb dip is now about 10%, so larger than in the case of OD. The dips are difficult to see because they are close together, and very broad.

The transition shown in fig. 4 is the  $Q_1(27)$  for which indeed only four strong hyperfine transitions are expected. In principle more hyperfine transitions are possible but the transitions with  $\Delta F \neq \Delta J$  are roughly a factor  $J^2$  weaker than the  $\Delta F = \Delta J$  transitions which means a factor  $J^4$  difference for the intensity of the Lamb dips. The observed splitting is of course a combination of the splitting in the excited and in the ground state. The splitting can, however, very well be explained by the splitting of the ground state only, using the constants for  $v'' = 0$ , as shown in fig. 4. This indicates that the splittings in the excited state are negligible for high  $J$  values. To check this, we also looked at the  ${}^PQ_{12}(28)$  which excites the same upper level, but starts from the other spin multiplet in the ground state,  $X^2\Pi_{3/2}$ , which has a much smaller hyperfine splitting than the  $X^2\Pi_{1/2}$  multiplet. As expected only one strong Lamb dip, consisting of several overlapping hyperfine components was observed. From such measurements we can give an upper limit of 15 MHz for the hyperfine  $b$  constant of the  $B^2\Sigma^+, v' = 0$  state.

It is seen in fig. 4 that the individual Lamb dips are quite broad ( $\approx 20$  MHz), which is due to the short radiative lifetime of the  $B^2\Sigma^+, v' = 0$  state. Other broadening effects are expected to be the same as for OD (about 1.5 MHz) and can therefore almost completely be neglected. It should be mentioned that cross-over resonances are not present as the transitions start all from different well separated levels in the ground state.

The linewidth  $\Delta\nu_{\text{tot}}$  (fwhm) for the highest and most isolated  $F' \leftarrow F''$  transition has been determined for several  $Q_1$  transitions. The  $Q_1$  transitions are chosen because these are the strongest ones with reasonably well separated hyperfine transitions. The line broadening  $\Delta\nu_\tau$  due to the natural lifetime can be deduced from the formula [16]

$$\Delta\nu_\tau = \Delta\nu_{\text{tot}} - (\Delta\nu_D^2)/\Delta\nu_{\text{tot}}, \quad (6)$$

valid for a convolution of a Lorentzian and a Gaussian line profile with linewidths (fwhm)  $\Delta\nu_\tau$  and  $\Delta\nu_D$ , respectively. In our experimental arrangement the (more or less) Gaussian contribution to the linewidth is only 1.5 MHz and consequently  $\Delta\nu_\tau \approx \Delta\nu_{\text{tot}}$ . The natural lifetime is determined via the relation  $\tau = 1/2\pi \Delta\nu_\tau$ .

In this way the natural lifetime of the  $N' = 16, F' = 18$  state in the  $B^2\Sigma^+, v' = 0$  state of  $\text{Si}^{35}\text{Cl}$  is determined as  $\tau = 10.0 \pm 1.5$  ns. A somewhat shorter lifetime of  $\tau = 7.8 \pm 0.7$  ns is found for the  $N' = 27, F' = 29$  state. If not shortened by predissociation, these lifetimes are determined by the coupling of the  $B^2\Sigma^+, v' = 0$  state with different vibrational-rotational levels in the  $X^2\Pi$  ground state only. In that case it can be compared with the lifetime that can be calculated from the measured electronic transition probability for the  $B^2\Sigma^+ \leftarrow X^2\Pi$  transition of  $\text{SiCl}$  [17], which also gives a lifetime in the order of 10 ns.

We also tried to resolve the hyperfine structure for transitions from low rotational levels, where the splitting is expected to be the largest. These transitions start, however, from rotational levels that are hardly populated in our beam [3], and are too weak to be detected by the Lamb dip technique. These transitions could, however, be observed in the second LIF region, where the molecular beam is better collimated. The linewidth of 30 MHz (fwhm) of single resolved hyperfine transitions is still mainly due to lifetime broadening. Therefore the loss in resolution by not using the Lamb dip technique is small in this special case. Resolved hyperfine transitions were observed whose splitting could be explained by the splitting in the ground state only. The observed splitting of the lowest rotational transitions is explicitly given in table 2. From these data an upper limit of 15 MHz was determined for the Fermi contact-term  $b_F = b + c/3$  in the excited  $B^2\Sigma^+, v' = 0$  state of  $\text{Si}^{35}\text{Cl}$ . These upper limits for the hyperfine coupling constants in the excited  $B^2\Sigma^+$  state indicate that there is only a small overlap of the electron spin distribution with the chlorine nucleus.

Furthermore from these measurements the sign of the hyperfine  $d$  constant in eq. (5) can unambiguously be determined. For the electronic transition under study the  $Q_1$  transitions probe upper  $A$ -doublet components whereas  $P_1$  and  $R_1$  transitions probe the lower  $A$ -doublet components of the ground state. From the observed hyperfine splittings it follows then that the hyperfine splitting in the upper  $A$  doublets is proportional to

$$[a - \frac{1}{2}(b+c)] + |d|(J + \frac{1}{2})$$

Table 2

Observed hyperfine splittings for the lowest rotational transitions of the  $B^2\Sigma^+$ ,  $v' = 0 \leftarrow X^2\Pi$ ,  $v'' = 1$  band of  $\text{Si}^{35}\text{Cl}$ . In the first column the rotational transitions are given, and the splitted hyperfine components are explicitly indicated. The observed splitting between these components is given in the next column. In the last column the calculated splitting between the hyperfine levels in the  $X^2\Pi$ ,  $v'' = 1$  state are given. These splittings are calculated according to eq. (5) using the hyperfine constants of ref. [15] for  $v'' = 0$

| Transition   | Observed splitting | Calculated splitting |
|--|--------------------|----------------------|
| ${}^{\circ}\text{Q}_{11}(1)$ $\left. \begin{array}{l} F' = 1, 2 \leftarrow F = 1 \\ F' = 1, 2 \leftarrow F = 2 \end{array} \right\}$       | $129 \pm 5$        | $\approx 128$        |
| ${}^{\circ}\text{R}_{21}(1)$ $\left. \begin{array}{l} F' = 0, 1, 2 \leftarrow F = 1 \\ F' = 1, 2, 3 \leftarrow F = 2 \end{array} \right\}$ | $122 \pm 6$        | $\approx 128$        |
| ${}^{\circ}\text{Q}_{21}(1)$ $\left. \begin{array}{l} F' = 1, 2 \leftarrow F = 1 \\ F' = 1, 2 \leftarrow F = 2 \end{array} \right\}$       | $\leq 20$          | $\approx 4.5$        |
| ${}^{\circ}\text{R}_{21}(1)$ $\left. \begin{array}{l} F' = 1, 2 \leftarrow F = 1 \\ F' = 1, 2, 3 \leftarrow F = 2 \end{array} \right\}$    | $36 \pm 5$         | $\approx 33$         |
| ${}^{\circ}\text{R}_{21}(1)$ $\left. \begin{array}{l} F' = 1, 2, 3 \leftarrow F = 2 \\ F' = 2, 3, 4 \leftarrow F = 3 \end{array} \right\}$ | $53 \pm 5$         | $\approx 62$         |
| ${}^{\circ}\text{P}_{12}(2)$ $\left. \begin{array}{l} F' = 1, 2 \leftarrow F = 1 \\ F' = 1, 2 \leftarrow F = 2 \end{array} \right\}$       | $34 \pm 4$         | $\approx 35$         |
| ${}^{\circ}\text{P}_{12}(2)$ $\left. \begin{array}{l} F' = 1, 2 \leftarrow F = 2 \\ F' = 2 \leftarrow F = 3 \end{array} \right\}$          | $39 \pm 4$         | $\approx 40$         |

and in the lower  $A$  doublets to

$$[a - \frac{1}{2}(b+c)] - |d|(J + \frac{1}{2}).$$

The sign as given in eq. (5) together with the phase convention for the  $A$  doubling as in ref. [3] implicates then that the  $d$  constant is positive. In their analysis of the microwave spectrum of  $\text{Si}^{35}\text{Cl}$  Tanimoto et al. [15] also assumed the  $d$  constant to be positive. Their Hamiltonian included however an extra minus sign in front of both the  $A$  doubling constants  $p, q$  and the hyperfine  $d$  constant. From their microwave spectra the absolute parities of the  $A$  doublet can, however, not be determined as the combinations  $(p, q, d)$  and  $(-p, -q, -d)$  yield the same result.

## 5. Conclusions

It is shown experimentally that the application of the Lamb dip technique to a wide and intense molecular beam makes a high spectral resolution possible. From increased widths of the Lamb dips it is also possible to determine accurately the natural lifetimes of excited states. Excited-state lifetimes that are in the order of 20 ns or shorter cannot be measured easily with pulsed lasers, as these lifetimes are in the order of the duration of the laser pulse, or because the spectral resolution of these lasers is poor. Especially in the region 0.1–20 ns, the Lamb dip technique works very well; the lifetime broadening is then so large that other broadening effects can be neglected. Furthermore the transitions to excited states with a short radiative lifetime are usually reasonably strong and saturation spectroscopy can be performed with moderate laser power densities. With the high spectral resolution required for the Lamb dip detection lifetimes of different quantum states can be measured separately.

## Acknowledgement

The authors wish to thank Messrs. L. Hendriks and E. van Leeuwen for their excellent technical assistance and Mr. J. Schleipen for his help with the data analysis. This work has been supported by the Stichting voor Fundamenteel Onderzoek der Materie (FOM) and has been made possible by financial support from the Nederlandse Organisatie voor Zuiver-Wetenschappelijk Onderzoek (ZWO).

## References

- [1] T. Kröckertskothén, H. Knöckel and E. Tiemann, *Chem. Phys.* 103 (1986) 335.
- [2] K.R. German, *J. Chem. Phys.* 64 (1976) 4192.
- [3] G. Meijer, B. Jansen, J.J. ter Meulen and A. Dymanus, *Chem. Phys. Letters* 136 (1987) 519.
- [4] W. Ubachs, J.J. ter Meulen and A. Dymanus, *Can. J. Phys.* 62 (1984) 1374.
- [5] W.A. Majewski, *Opt. Commun.* 45 (1983) 201.
- [6] M.A.A. Clyne, J.A. Coxon and A.R. Woon Fat, *J. Mol. Spectry.* 46 (1973) 146.
- [7] T. Bergman, P. Erman, Z. Haratym and M. Larsson, *Physica Scripta* 23 (1981) 45.
- [8] W.L. Meerts and A. Dymanus, *Astrophys. J.* 180 (1973) L93.
- [9] K. Shimoda, ed., *Topics in applied physics, Vol. 13. High-resolution laser spectroscopy* (Springer, Berlin, 1976).
- [10] W. Ubachs, Ph.D. Thesis, Nijmegen (1986).
- [11] R.A. Frosch and H.M. Foley, *Phys. Rev.* 88 (1952) 1337.
- [12] J.A. Coxon, *J. Mol. Spectry.* 58 (1975) 1.
- [13] G.C. Dousmanis, T.M. Sanders Jr. and Ch. Townes, *Phys. Rev.* 100 (1955) 1735.
- [14] J.M. Brown, I. Kopp, C. Malmberg and B. Rydh, *Physica Scripta* 17 (1978) 55.
- [15] M. Tanimoto, S. Saito, Y. Endo and E. Hirota, *J. Mol. Spectry.* 103 (1984) 330.
- [16] S.N. Dobryakov and Y.S. Lebedev, *Soviet Phys. Doklady* 13 (1969) 873.
- [17] A.V. Mandrugun, L.A. Kuznetsova and Yu.Ya. Kuzyakov, *Spectry. Letters* 17 (1984) 259.